ELSEVIER

PII: S0021-9290(96)00095-4

J. Biomechanics, Vol. 30, No. 1, pp. 49–56, 1997

Printed in Great Britain
0021-9290/97 $17.00 + .00

MODELLING MUSCLE ACTIVITY IN STANDING WITH CONSIDERATIONS FOR BONE SAFETY

Marko Munih* and Alojz Kralj

Faculty of Electrical Engineering, University of Ljubljana, Ljubljana, Slovenia

Abstract—The functional use of electrical stimulation (FES) for the restoration of movement to paraplegics has been improved in the last decade but questions about the mechanical effect of stimulation on the skeleton have arisen. In intact people, neuromuscular activity not only controls movement, but also minimizes bone and joint tissue loading. Current FES systems do not use feedback and do not even use average natural patterns of muscle activation. FES systems would be safer if muscle activation patterns were synthesized so as to minimize bending in the long bones.

By modelling, we have verified that appropriate muscular activity reduces bone bending stresses, an approach we named active unloading of the skeleton. Using this criterion for control is novel. The muscle activation was calculated using measurements from intact people in different postures, and later modelling of the musculoskeletal system. The two-dimensional model of the lower limb includes 23 muscles relevant primarily for movement in the sagittal plane. The muscle model for constraint calculation is divided into first-order activation dynamics and first-order contraction dynamics. Optimization, which includes minimization of net bending moment calculated along the long bones, is static because changes in the observed postures are slow.

In the calculated muscle activity patterns, muscle coactivation and cocontraction yield very uniform and low bone loading. Net bending moment values were fairly stable as the posture varies. The moment distribution in the femur was found to be U-shaped, while in the tibia it is sometimes V-shaped. The bones are naturally thicker at the points of peak moment. Copyright © 1996 Published by Elsevier Science Ltd.

Keywords: Muscle forces; Bending moment; Synergism; Standing; Musculo–tendino-skeletal model.

NOMENCLATURE

F_T, F_{Tj}, $\tilde{F}_T$	absolute, individual and normalized tendon force
$\tilde{F}_{CE\,iso}$	isometric force–length relation of CE
F_{Tmin}, F_{Tmax}	minimal and maximal tendon force
F_0, F_g	active muscle maximal force and gravity force
M_g, M_n	gravitational and net bending moment
$\tilde{M}_{mn}$	normalized array of muscle bending moments (m)
M_{Li}, M_{Gi}	ligament and gravitational moments in joints (i = hip, knee, ankle)
l_{M0}	muscle length at maximal force
$\tilde{l}_M$, $\tilde{l}_{MT}$	muscle and muscle–tendon normalized lengths
v_{max}	maximal muscle velocity
$\tilde{v}_M$, $\tilde{v}_{MT}$	muscle and muscle–tendon normalized velocities
$\tilde{k}_{PE}$	normalized PE element stiffness
r_g, r_m, r_{ij}	moment lever for M_g, $\tilde{M}_{mn}$ calculation and muscle levers in joints
u	central neural excitation
a	muscle activation
FC	muscle fibre composition
α	muscle pennation
q	muscle attachment variable

INTRODUCTION

Contrast two muscle activation schemes which are used in FES today. (i) Simple stimulation patterns include two-channels of bilateral *m. quadriceps* for standing. For four-point walking, two additional channels are used for *Peroneal nerve* stimulation, which triggers the flexion reflex to activate the swing phase of gait (Kralj and Bajd, 1989). (ii) More complex walking with 32 channels of percutaneous electrode stimulation (in a laboratory environment) offers improved locomotor function and movement elegance (Marsolais *et al.*, 1991). Although stimulation may be based upon EMG patterns from intact people, no formal optimization procedure has been presented. The main shortcomings of this approach are (i) that repeated use of the same muscles result in fatigue and (ii) that in safe systems one should not neglect the fact that a plegic person is biomechanically very different from an intact person and therefore, designers of artificial control systems should, in addition to functional needs, consider the safety of the skeleton. The simple open-loop four-channel stimulation, used today in Ljubljana and other centres, should be examined with regard to the mechanical loading effects of muscle activity induced by stimulation; in this respect, control methods remain unsatisfactory.

Safety in an open- or closed-loop FES system relies, for protection of the bone, as in nature, on limiting the loading. The muscle–bone unloading principle was first recognized by Pauwels (1965), who studied the construction of the human biomechanical system and the influence of muscle activity on bone and joint mechanical loading. He exposed fundamental biomechanical rules showing that muscle action not only provides moments for stability and movement generation, in one or several dynamically coupled joints, but, generally, loads the bone with compressive, tensile and shear stresses. Compressive and tensile stresses consist of (i) a pure compressive/tensile component produced by axial force and (ii) a bending moment component produced by a loading force positioned outside of the bone centre. The shear, and

Received in final form 14 *May* 1996.

* Address correspondence to: Marko Munih, D.Sc. Faculty of Electrical Engineering, University of Ljubljana, Trzaska 25, 1000 Ljubljana, Slovenia.

more especially the bending component, are dangerous for bone, because stresses can exceed those during pure axial loadings by factors of several decades (30–50; Biewener, 1991). Shear stresses should be avoided, because bone structure is adapted to carry compressive and tensile stresses but not shear (Currey, 1970; Reilly and Burstein, 1975). Fortunately, appropriate muscle action can, in addition to maintaining joint moment equilibrium, also minimize the bending moment of the bone (Bertram and Biewener, 1988; Pauwels, 1965), producing a more consistent distribution of stress in a bone during locomotion (e.g. Rubin and Lanyon, 1982). The bending-induced strains are the worst-case loading situation for the limb bones; the proportion of strain due to bending has been experimentally verified to be up 24 times the strain due to axial loading for some animals (e.g. Alexander, 1974; Biewener *et al.*, 1983; Lanyon and Bourn, 1979).

By using active unloading, the bending moments along the bones are minimized by transforming the bending loads into pure compressive loads. This is achieved by reducing the external bending moment, which is produced by gravitational and other external forces, with an appropriate combination of muscle forces. These forces result in bending loads of opposite sign which in total put the bone into pure compression. With this technique, adequate muscle action may double the compressive load but the bending moment is minimized (Pauwels, 1965). The implementation of the minimal bending moment criterion results not only in minimal long bone stress, but also selects synergistic muscle activity characteristic of natural muscular activity.

Due to the redundancy of the muscle–joint system, muscle forces in general cannot be directly calculated from the external joint moments. To solve such an indeterminate problem, either static optimization for slow movements or dynamic optimization for fast responses is possible. Static optimization techniques require a cost function which is usually a combination of muscle size, force or stress, activation level and muscle fatigue. The solution is not dependent on other factors but is, of course, limited by its failure to account for the dynamic properties of real muscles (Khang and Zajac, 1989). Dynamic optimization, though requiring much more computation, can improve performance, but a dynamic scheme requires several optimizations to be performed at real-time speeds which are beyond current software and hardware capabilities. On the other hand, computer procedures for static optimization are realizable and well-suited to the requirements for this study of standing.

Many researchers have dealt with lower extremity models: from the complex static or dynamic cost functions of Chow and Jacobson (1971), through the comprehensive models of Hatze (1981), to the work of Zajac and coworkers (Khang and Zajac, 1989; Yamaguchi and Zajac, 1990), to mention only some of them. However, few studies considered either the joint or bone safety aspects of the musculoskeletal system. For example, Seireg and Arkivar (1973) used different static optimization functions to study standing with (i) minimized sum of three-dimensional passive moments in ankle, knee and hip joints and (ii) minimized sum of vertical reactions in ankle, knee and hip joints. Because of the good correspondence with EMG recordings, the same authors (Seireg and Arkivar, 1975) again used minimization of passive moments in a study of walking. In contrast, femur and tibia safety was only considered and studied in Pauwels' work in 1965. Even there, Pauwels used safety principles from theoretical analysis of the loading and not to synthesize the muscular activity.

MODELLING

The sagittal plane model of standing was divided into three parts: segmental kinematics, musculoskeletal geometry and musculotendon actuator dynamics. Minimal and maximal constraints for muscle forces were determined by forward integration of the dynamic musculotendon actuator model, and then actual muscle forces were determined via static optimization and the inverse dynamics. The safety criterion was a static optimization cost function which minimized the long bone (femur and tibia) bending moments: this distributed the external load among several active muscles. Ligament constraint moments are included in the ankle, knee and hip equilibrium equations. Prior to the force optimization, the gravitational and normalized muscular bending moments were calculated. The modelling is based on cadaver data, linearly scaled to the subject's anthropometric dimensions (Munih and Kralj, 1992). Posture and support forces during standing were assessed in the laboratory as described in the measurement section.

Segmental kinematics

The body was divided into seven segments (Fig. 1): the lower segments represented the left and right feet (mass concentrated in appropriate mass centre points), left and right shanks and left and right thighs, with mass distributions modelled as truncated cones. The rest of the body including pelvis, trunk, head and both arms are brought together in a single mass centre located in the trunk (Contini, 1972; Drillis and Contini, 1966; Winter, 1979). The body was assumed to be symmetrical about the midline. The thigh and shank masses were distributed along the segments to minimize the error from gravitational forces on the bending moments determined for these segments. The artificial radii, for the truncated cone, representing thigh and shank, were calculated according to segment length, mass and density.

Segment kinematics was modelled by homogeneous transformations (Paul, 1982). The coordinate system for the shank, thigh and the rest of the body were positioned in ankle, knee and hip rotation centres respectively, while the coordinate system for each foot was the same as for the ipselateral shank. The joint rotation centres were determined as previously reported (Munih and Kralj, 1992). The ankle and hip joints were considered as rotational, one-degree-of-freedom joints, while the knee joint also included translation through the evolute curve (Maquet, 1984).

Musculoskeletal geometry

The musculoskeletal geometry determines how the muscle forces are converted into muscle moment. Two approaches are possible: (i) as a straight line between two attachments or (ii) as a centroid line. The centroid line is

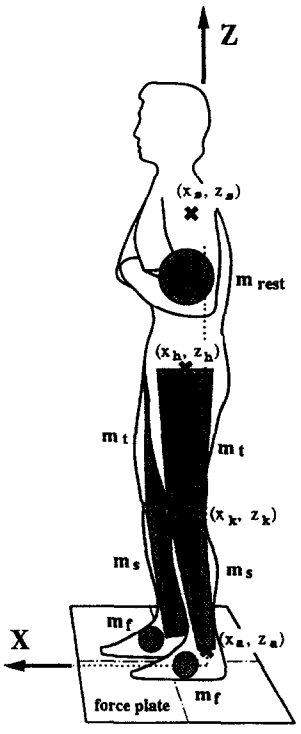

Fig. 1. Schematic representation of the posture of a subject on the force plate with four markers attached at the ankle (x_a, z_a), knee (x_k, z_k), hip (x_h, z_h) and shoulder (x_s, z_s) joints. The segment masses: m_f for feet, m_s for shank, m_t for thigh and m_{rest} for head, ankle and trunk are also displayed. m_f and m_{rest} are modelled as point masses, while m_s and m_t are modelled as truncated cones.

generally found by virtually cutting the muscle into slices transverse to the muscle fibres' direction, and connecting the centres of each slice along the length of the muscle. Then the shortest distance from the point on the middle line of the bone to the curve passing through the centroids of the muscle represents the moment lever. The centroid line is accurate for the calculated posture, but may change grossly by varying the body position. The difference between the computationally more complex centroid line method and the straight-line approach is between 1 and 12% according to data in the literature (Jensen and Davy, 1975). Based on these observations, the straight-line approach was used in this study.

The muscle attachment shapes were divided geometrically into three different groups, as in our previous study (Munih and Kralj, 1992), in which three-dimensional numerical muscle and bone data were collected from a 26 year old male cadaver. Twenty-three muscles relevant for movements in the sagittal plane were considered: *m. sartorius, m. gracilis, m. semitendinosus, m. gluteus maximus, m. tensor fasciae latae, m. biceps femoris longus, m. biceps femoris brevis, m. gluteus medius*, m. adductor magnus*, m. rectus femoris*, m. vastus intermedius, m. vastus lateralis, m. vastus medialis, m. iliacus, m. psoas major, m. adductor longus, m. semimembranosus, m. gastrocnemius*, m. soleus*, m. tibialis anterior, m. peroneus longus, m. peroneus brevis, m. digitorum longus.* Because of their morphology, the muscles marked with an asterisk were divided into two separate parts.

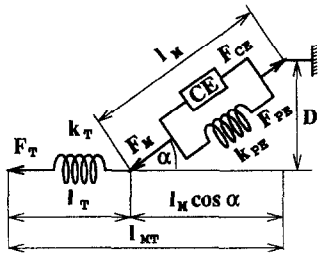

Fig. 2. Musculotendon contraction model including tendon (T), contractile and passive element (CE, PE) with uniform pennation angle.

Musculotendon actuator dynamics

The optimization procedure must take into account several physical constraints, including a minimum, $F_{T\min}$, due to elasticity of the muscle when there is no activation, and maximum, $F_{T\max}$, range of muscle forces (e.g. Dul *et al.*, 1984a, b; Seireg and Arkivar, 1973, 1975). Usually, in static optimization, it is assumed that physiological or anatomical muscle cross sections have some typical maximal stress value and this is used to determine the maximal possible muscle force. Such an approach excludes the static or dynamic properties of tendon and muscle. In contrast, dynamic models frequently use high-order linear differential equations to describe the muscle–tendon properties (Chow and Jacobson, 1971; Hatze, 1981; Khang and Zajac, 1989; Yamaguchi and Zajac, 1990). The fact that the muscles cannot generate force instantaneously should also be considered, and that lead us to use a simple dynamic muscle modelling approach for determining $F_{T\min}$ and $F_{T\max}$.

Hill's musculotendon model was implemented in a way similar to that used recently by Zajac (1989) and Winters and Stark (1985) (Fig. 2). The central neural system excitation u acts through a first-order activation dynamics, generating an internal muscle state called muscle activation which triggers muscle cross-bridge force development, through the contraction dynamics. The activation dynamics were modelled as muscle-independent single-input–single-output (SISO) (Zajac, 1989) with an activation time constant of 20 ms and a deactivation time constant equal to 200 ms. With FES, the system excitation u is a function of three stimulation parameters: amplitude, pulse width and frequency but these effects lumped together within the input variable u.

The dimensionless musculotendon contraction dynamics includes the active and passive properties of tendon (T), a contractile element (CE) and a passive element (PE) (Fig. 2). The series elasticity of CE was neglected since it is of little significance in the dynamics of FES standing (Zajac, 1989). All absolute parameters in the model were scaled according to the muscle length l_{M0} at maximal muscle force, maximal muscle velocity v_{max} and active muscle maximal force F_0 (normalized variables are marked with $\sim$). The force–length relation $\tilde{F}_{CE\,iso}(\tilde{l}_M, a)$ of the CE element was modelled after Hatze (1976), while force–velocity of CE was taken as Hill's relation for $\tilde{v}_M > 0$ and as FitzHugh (1976) for $\tilde{v}_M < 0$ where shape and v_{max} vary with muscle fibre composition (Winters and Stark, 1988). The parallel elasticity ($\tilde{k}_{PE}$) greatly influences the model output force and is defined for all

muscles as in Stephenson and Williams (1982). The tendon was assumed to be elastic and linear with $\varepsilon_0 = 0.033$ at $F_T = F_0$ (stress equal to 32 MPa) (Zajac, 1989). Given all those muscle properties, the first-order contraction dynamics was defined as

$$\frac{d\tilde{F}_T}{dt} = f(\tilde{F}_T, \tilde{l}_{MT}, \tilde{v}_{MT}, a, \alpha, FC). \quad (1)$$

With the exception of the few details described above, our musculotendon model is similar to that used by Pandy *et al.* (1990). In static conditions, $u = 0$ gives $F_{T\min}$ and $u = 1$ gives $F_{T\max}$.

Bending moments

Two different types of bending moment were calculated for each time sample: (i) gravitational bending moments M_g (caused by the ground reaction force and gravity) and (ii) normalized muscle bending moments $\tilde{M}_{mn}$ (caused by muscular activity).

The gravitational bending moments M_g were determined as $M_g = F_g r_g$. The lever r_g represented distance from the force vector to the calculated central point in bone and the gravity force F_g was derived from segment anthropometric data and ground reaction force vector which was measured in the laboratory.

The normalized bending moment $\tilde{M}_{mn}$, for each selected muscle, was determined as the bending moment for 1 N tendon force ($\tilde{M}_{mn} = F_T r_m q$; $F_T = 1$ N), where r_m represents the distance from the tendon force vector to the calculated central point in the bone. Special attention was paid to the muscle tendon force value in the regions of the origin and the insertion (Fig. 3). While calculating $\tilde{M}_{mn}$, in these regions, only part of the whole muscle–tendon force, depending on current position inside the attachment area, loads the bone. This is included through attachment variable $0 \leqslant q \leqslant 1$, as the origin and insertion move along the attachment regions.

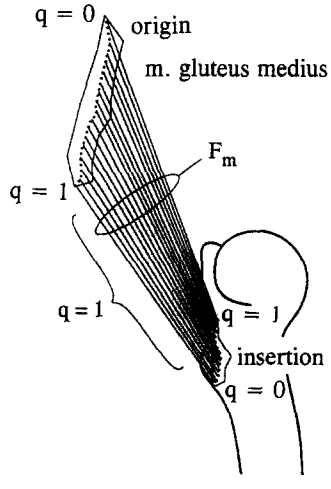

Fig. 3. $\tilde{M}_{mn}$ calculation could be divided into two different regions. Between muscle origin and insertion $F_T = 1$ N produces $\tilde{M}_{mn}$. Within the origin and insertion regions (insertion in this figure), only part of F_T, determined with variable q, produces $\tilde{M}_{mn}$. q changes with the current calculation point according to the percentage of force loading area.

Optimization

The normalized muscular bending moments $\tilde{M}_{mn}$ should be combined in such a way that gravitational bending moments M_g are minimized:

$$J = |\tilde{M}_{mn} F_T - M_g| \quad (2)$$

with solution space constrained:

$$F_{T\min} \leqslant F_T, \qquad F_T \leqslant F_{T\max}. \quad (3)$$

As some muscles are divided into two independent parts, the number of inequalities is doubled (to 56) with respect to the number of muscles. Additionally, the following three moment equilibrium equations (i = hip, knee, ankle) must be satisfied:

$$\sum_{j=1}^{28} r_{ij} F_{Tj} + M_{Li} + M_{Gi} = 0. \quad (4)$$

The muscle levers r_{ij} were determined according to the subject's posture. The ligament moments in the joints M_{Li}, which were most important at extreme joint angles, were modelled after Hatze (1976). M_{Gi} represents the gravitational moment in the joints. For finding the optimally constrained solution of equation (2), the least-squares error method with Kuhn–Tucker conditions was used (Lawson and Hanson, 1974).

MEASUREMENTS

In addition to the anthropometric muscle and bone data, the subject's posture data and ground reaction vector (GRV) are needed to calculate the position of body masses. These were measured in the sagittal plane for five normal subjects (men, 24 to 27 years) in the laboratory in various standing postures. An AMTI (Advanced Mechanical Technology Inc.) strain gauge force plate (ORG6-5-1) was used to assess GRV amplitude and position. The positions of four body markers placed on the shoulder, hip (trochanter major), knee, and ankle were acquired with OPTOTRAK (Northern Digital Inc.) measuring system. The subjects stood upright, with hands crossed on the chest, heels placed together, while the angle between the feet was approximately 30°. Various measurement protocols were examined in each person. In one, shown in the results section, the subject assumed a normal standing posture for 10 s, then leant forward for 10 s, leant backward for 10 s and, finally concluded with 10 s in normal standing. This protocol was chosen with regard to quiet standing and posture switching dynamics. The forward/normal/backward inclination moved the GRV position typically 11/5/0 cm in anterior/posterior direction; the shoulder position typically in the range of 12/0/ − 7 cm; the hip typically 12/6/5 cm, while the ankle position stayed at the reference (0 cm).

RESULTS

The figures show a detailed study of one simulation run for a single person (Figs 4–6) and the comparison of net bending moments in different persons (Fig. 7).

Figure 4 shows typical time courses for the calculated muscle activity in a single subject. Even if the posture

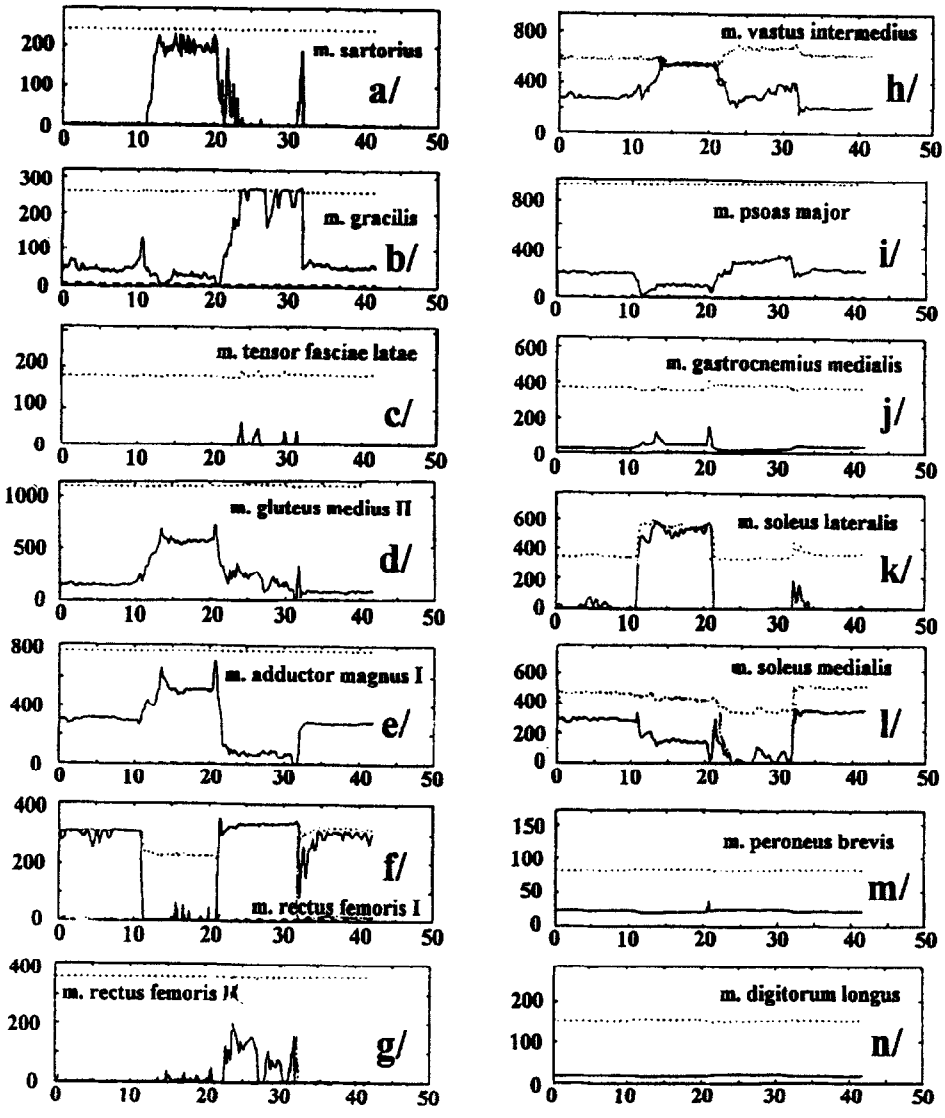

Fig. 4. Muscle force during switching posture in standing. Vertical axis represents the tendon force in (N), horizontal axis is time in (s). Solid line represents the bending optimized tendon force F_T, dotted line F_{Tmax}, dashed line F_{Tmin}. Values for F_{Tmin} are usually small and thus invisible, except in this case in muscles: *m. gracilis, m. rectus femoris.*

deviations from upright standing are relatively small, when compared to normal standing, it is obvious that the maximal tendon force F_{Tmax} (dotted line in Fig. 4) effects all muscles forces during postural changes. Major changes can be observed especially in *m. rectus femoris I*, *m. vastus intermedius*, and *m. soleus*. In *m. gracilis*, the dashed line represents minimal tendon force F_{Tmin}. For all the other muscles, F_{Tmin} were also calculated, however they are not visible in the figure because of their low value. By comparing the calculated tendon forces (solid line in Fig. 4), it is obvious that force is modulated simultaneously in several muscles at the same joint. This represents synergistic muscle activation in the coactivation and cocontraction sense (Dul *et al.*, 1984a, b; Herzog and Leonard, 1991; Winter, 1987). Coactivation occurs when several muscles work together to produce higher joint moment, while cocontraction means cooperation of agonist and antagonist muscle. At the hip joint the following muscles work together: *m. sartorius*, *m. gracilis* and *m. rectus femoris I* to produce hip flexion, while *m. gluteus medius II*, *m. psoas major* and *m. adductor magnus I* work to generate hip extension torque. A similar situation is found at the ankle joint where *m. soleus* (*lateralis* and *medialis*) works together with *m. gastrocnemius medialis* to pull the body back, while *m. peroneus brevis* and *m. peroneus longus* try to pull the standing body forward.

After the forces were known, the inverse muscular activation dynamics was used to calculate the neural activity. In standing, the relatively fast activation/deactivation time constants (20 ms/200 ms) cause the shape of the neural activity u to be similar to the force curves.

The muscle activity shown in Fig. 4 generates loading and unloading bending moments described as $\tilde{M}_{mn}$ in the femur and tibia. These 'active' bending moments add to the gravitational bending moments M_g to produce net bending moments $M_n(M_n = \tilde{M}_{mn}F_T + M_g)$ which stresses the bones. In Figs 5 and 7, the diagram always represents the bending moment M_n, determined in 50 ms

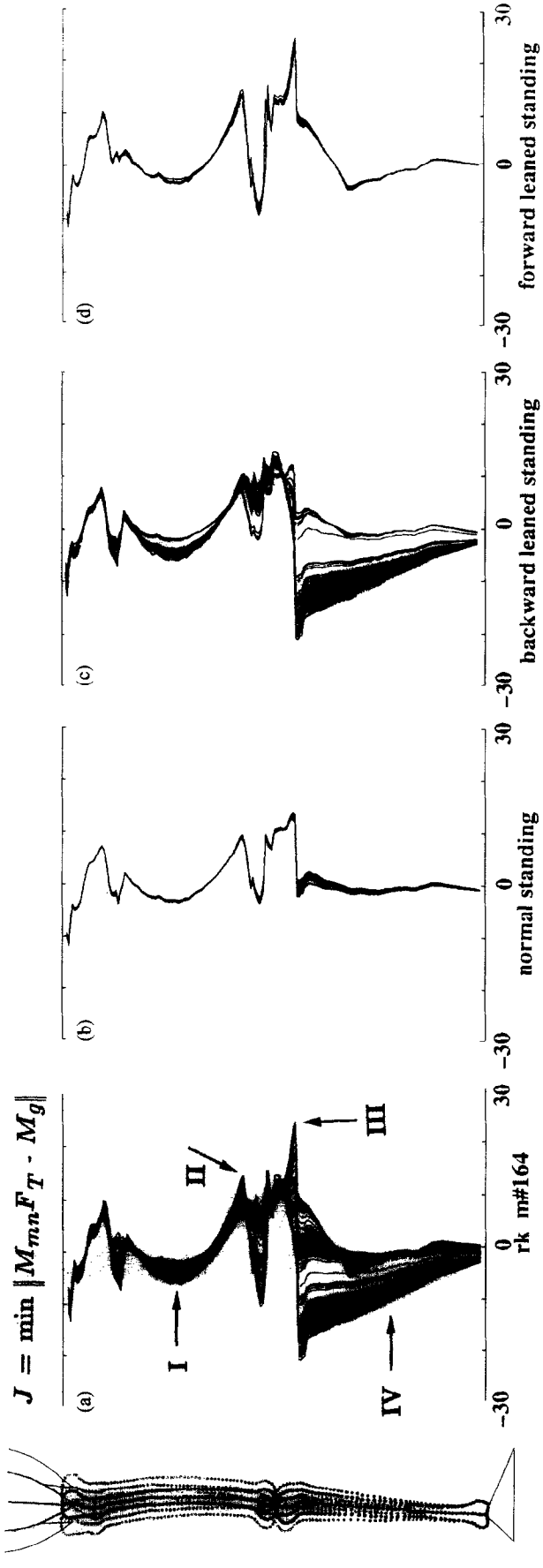

Fig. 5. Detailed measurements in single person. Horizontal axis shows M_n bending moment as it appears in calculated central points of the bone. Due to calculation in intervals several lines are visible.

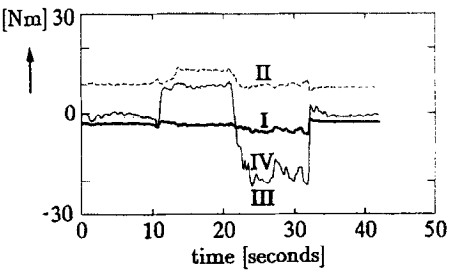

Fig. 6. Net bending moments at particular high-stress and other selected points vs time for minimized bending loading. The points I, II, III and IV are selected as is shown in Fig. 5(a).

discrete time intervals, each being represented with one curve. Fig. 5(a) shows the whole measurement period including all standing postures (as in Fig. 4): Fig. 5(b) shows only the time interval when the person was in the normal-standing position; Fig. 5(c) the period of backward-standing; and Fig. 5(d) the period of forward-standing. The moments in normal standing appear to be very uniform, which seems logical. In all diagrams for the femur, the bending moment distribution appear to be U-shaped, while along the tibia, higher bending moment amplitudes, with a triangular V-shaped distribution appear for backward-standing posture (Fig. 5(c)). Since the peak values are of the greatest concern for safety, Fig. 6 shows the time courses M_n at particular selected points. The most extreme values occur at switching events, remain fairly high at 'extreme' body positions and are very low during normal standing (which is almost amuscular, as we can see in Fig. 4).

Figure 7 shows the net bending moments M_n for four additional male subjects. The curve shapes show no essential difference compared to Fig. 5. Discrepancies among persons exist and can be attributed to the more or less rapid movements between different standing phases. The shape of moment M_n is similar in all cases and does not change significantly among different persons, even if all anthropometrical and geometrical coordinates were scaled according to the individual.

DISCUSSION

In this study equal importance was given to achieving joint moments and to the bone bending moments. Some new techniques have been introduced in the modelling. Even in simple activities such as standing and posture switching, the results suggest that it is essential to allow variations in the boundaries $F_{T\,min}$ and $F_{T\,max}$ in order to obtain accurate results. For example, Fig. 4 shows pronounced modulation of both upper and lower tendon force constraints, originating primarily from variable musculotendon actuator length. Further simplification by making $F_{T\,min}$ and $F_{T\,max}$ constants, as has often been described in the literature, would lead to poorer accuracy.

The synergistic muscle activation, found in all our simulations, is characteristic of natural muscular activity (Herzog and Leonard, 1991; Pedotti *et al.*, 1978). We have found that if minimization of bone bending moment

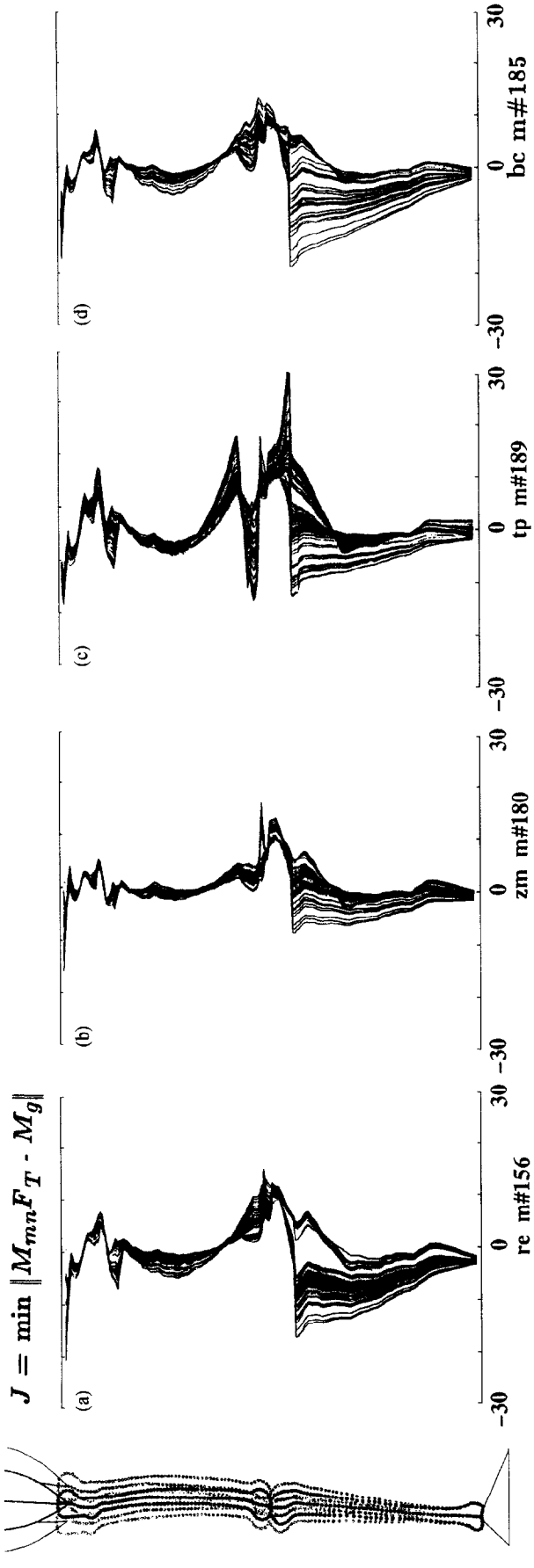

Fig. 7. Net bending moment M_n in four intact persons.

is incorporated, synergistic muscle coactivation and cocontraction results. In contrast, several past studies have used various artificially created high-order optimization functions in order to add muscle synergism into the model (Dul *et al.*, 1984a, b; Herzog and Leonard, 1991). The synergistic activity may incorporate coactivation and cocontraction. Coactivation in general, leads to minimal energy consumption with several submaximally activated muscles, generating together higher joint moment, which might be otherwise achieved with only one maximally activated muscle. However, as the energy consumption relates to the second or third power of muscle force (Crowninshield and Brand, 1981) and because the total muscle fatigue and energy consumption are added from all the muscles, it is more economical to use several muscles at low activation instead of one muscle at a high activation (e.g. $\Sigma F_i^3 < F^3$ if $\Sigma F_{ii} = F, F_i > 0$). The coactivation leads to smaller energy consumption and lower muscle fatigue. Note that neither the energy consumption nor the consequent muscle fatigue have been made a criterion for optimization: rather, their reduction results from the minimization of the loading of the bone.

When studying the shape of the bending moment along femur and tibia, it can be observed that net bending moment agrees with the theoretical predictions of Pauwels (1965), regardless of the subjects' postures. Pauwels predicted higher moment values with triangular shape in the tibia for forward-leaning postures: this is verified by Fig. 5(d). Also, higher values of M_n, with a V-shape in the tibia, are mostly found in backward standing (Fig. 5(c)). The reason for these characteristic profiles for the bending moments, originates in the musculoskeletal system, and could be described as follows. The net bending moment M_n is the sum of the gravitational moment M_g and the combined muscular bending moments $\tilde{M}_{mn}F_T$. For the tibia, the triangular muscle moment distribution, with higher value at the ankle joint, could be found for each of the active muscles: *m. soleus*, *m. peroneus brevis* or *m. peroneus longus* (Fig. 4). This means that there is no muscle which could biomechanically compensate for a rectangular or a triangular shape of M_g with higher moment at the knee. The distribution and magnitude of the moment is not critical because backward leaning is unnatural and rarely used. The knee moment in this case must be balanced by *m. quadriceps* activity.

Additional information about the bone loading mechanism is evident from Fig. 6, which demonstrates that the peaks in the minimized bending moment appear only in bone regions with enlarged cross-sectional area. Higher moment values are observed in Fig. 6, also in the middle sections of the bones. Further estimation of the real stresses is beyond the scope of this paper and any calculations of stresses, based on these bending moments and without detailed bone data, would be speculative. In general, higher bending moments result in an increase of stress value, but the bone deformations are plastic, not according to Hook's law.

Comparing M_n for several persons, no significant difference can be seen after the minimal bending criterion has been applied. The variations of moment amplitudes are expected because of differences in skeletal geometry and body segment masses. However, they still remain in

the same amplitude range even though posture changing was subjective.

CONCLUSIONS

We have shown that appropriate muscular activity can not only provide the joint moments required for standing, but can do so with small stresses in the long bones and thus improve safety. The modelling results show that this is achieved by a synergistic sharing of the external load among the muscles. Both coactivation and cocontraction have been found. Variations in the optimized loadings are small among different persons in similar postures. It can be concluded that the 'unloading principle' is useful. We expect that the same would be true for other normal activities such as standing up, stepping, etc.

Although the results are not shown here, we also found that the active unloading of the skeleton produces smaller bending loads in the long bones than currently used simple four-channel FES stimulation sequences. This is primarily due to the larger number of active muscles which can compensate for moment peaks in intact persons. Even higher loading was found when paraplegics stood in extreme forward or backward postures, assisted by FES of a small group of muscles. Only with a sufficient number of stimulated muscles, using multichannel devices with sophisticated muscle force control, might we be able to achieve loadings similar to intact persons. At present, use of the proposed optimization in real-time seems to be unrealistic: the large number of force sensors (about 10, see Fig. 4) required for practical implementation cannot easily be implemented with current implant technology. However, the method is useful for generating activation patterns to be applied open-loop with multielectrode implants.

Acknowledgements—This study was supported in part by Research Grant No. H 133G00151 from the NIDRR, Washington D.C., and Ministry of Science and Technology, Ljubljana, Slovenia. The authors also thank Prof. Tadej Bajd, D.Sc. for their constructive suggestions during the study and Dr Nick Donaldson for his suggestions during the manuscript preparation.

REFERENCES

Alexander, R. M. (1974) The mechanics of a dog jumping (*Canis familiaris*). *J. Zoology* **173,** 549–573.

Bertram, J. E. A. and Biewener, A. A. (1988) Bone curvature: sacrificing strength for load predictability. *J. Theoret. Biol.* **131,** 75–92.

Biewener, A. A. (1991) Musculoskeletal design in relation to body size. *J. Biomechanics* **24,** 19–29.

Biewener, A. A., Thomason, J. J. and Lanyon, L. E. (1983) Mechanics of locomotion and jumping in the forelimb of the horse (Equus): *in vivo* stress developed in the radius and metacarpus. *J. Zoology* **201,** 67–82.

Chow, C. K. and Jacobson, D. H. (1971) Studies of human locomotion via optimal programming. *Math. Biosci.* **10,** 239–306.

Contini, R. (1972) Body segmental parameters. Part II. *Artificial Limbs* **16,** 1–19.

Crowninshield, R. D. and Brand, R. A. (1981) A physiologically based criterion of a muscle force prediction in locomotion. *J. Biomechanics* **14,** 793–801.

Currey, J. D. (1984) *The Mechanical Adaptations of Bone.* Princeton University Press, Princeton, NJ.

Drillis, R. and Contini, R. (1966) Body segmental parameters. Report No. 1163-03, Office of Vocational Rehabilitation, Department of Health and Education and Welfare, New York.

Dul, J., Townsend, M. A., Shiavi, R. and Johnson, G. E. (1984a) Muscular synergism—I. On criteria for load sharing between synergistic muscles. *J. Biomechanics* **17,** 663–674.

Dul, J., Johnson, G. E., Shiavi, R. and Townsend, M. A. (1984b) Muscular synergism II. A minimum-fatigue criterion for load sharing between synergistic muscles. *J. Biomechanics* **17,** 675–684.

FitzHugh, R. (1977) A model of optimal voluntary muscular control. *J. Math. Biol.* **4,** 203–236.

Hatze, H. (1976) The complete optimization of human motion. *Math. Biosci.* **28,** 99–135.

Hatze, H. (1981) *Myocybernetic Control Models of Skeletal Muscle: Characteristic and Applications.* University of South Africa, Pretoria.

Herzog, W. and Leonard, T. R. (1991) Validation of optimization models that estimate the forces exerted by synergistic muscles. *J. Biomechanics* **24,** 31–39.

Jensen, R. H. and Davy, D. T. (1975) An investigation of muscle lines of action about the hip: a centroid line approach vs the straight line approach. *J. Biomechanics* **8,** 103.

Khang, G. and Zajac, F. E. (1989) Paraplegic standing controlled by functional neuromuscular stimulation. Part I—Computer model and control-system design. *IEEE. Trans. biomed. Engng* **36,** 873–884.

Kralj, A. and Bajd, T. (1989) *Functional Electrical Stimulation: Standing and Walking After Spinal Cord Injury.* CRC Press, Boca Raton, FL.

Lawson, C. L. and Hanson, R. J. (1974) *Solving Least Squares Problems.* Prentice-Hall, Englewood Cliffs, NJ.

Maquet, P. G. J. (1984) *Biomechanics of the Knee.* Springer, Berlin.

Marsolais, E. B., Kobetic, R., Chizeck, H. J. and Jacobs, J. L. (1991) Orthoses and electrical stimulation for walking in complete paraplegia. *J. Neurol. Rehabil.* **5,** 13–22.

Munih, M. and Kralj, A. (1992) Bending moments in lower extremity bones for two standing postures. *J. biomech. Engng* **14,** 293–302.

Munih, M., Kralj, A. and Bajd, T. (1995) Calculated muscle activity during paraplegic standing optimised for minimal femur and tibia bone loading, *BES Symp. on electrical stimulation—clinical systems,* pp. 73–74. Glasgow.

Pandy, M. G., Zajac, F. E., Sim, E. and Levine W.S. (1990) An optimal control model for maximum-height human jumping. *J. Biomechanics* **23,** 1185–1198.

Paul, R. P. (1982) *Robot Manipulators: Mathematics, Programming, and Control.* MIT Press, Cambridge.

Pauwels, F. (1965) *Gesammelte Abhandlungen zur funktionellen Anatomie des Bewegungsapparates.* Springer, Berlin.

Pedotti, A., Krishnan, V. V. and Stark, L. (1978) Optimization of muscle-force sequencing in human locomotion. *Math. Biosci.* **38,** 57–76.

Reilly, D. T. and Burstein, A. H. (1975) The elastic and ultimate properties of compact bone. *J. Biomechanics* **8,** 393–405.

Rubin, C. T. and Lanyon, L. E. (1982) Limb mechanics as a function of speed and gait: a study of functional strains in the radius and tibia of horse and dog. *J. Exp. Biol.* **101,** 187–211.

Seireg, A. and Arkivar, R. J. (1973) A mathematical model for evaluation of forces in lower extremities of the musculo-skeletal system. *J. Biomechanics* **6,** 313–326.

Seireg, A. and Arkivar, R. J. (1975) The prediction of muscular load sharing and joint forces in the lower extremities during walking. *J. Biomechanics* **8,** 89–102.

Stephenson, D. G. and Williams, D. A. (1982) Effects of sacromere length on the force–Ca relation in fast and slow twitch skinned muscle fibers from the rat. *J. Physiol.* **333,** 637–653.

Winter, D. A. (1979) *Biomechanics of Human Movement.* Wiley, New York.

Winter, D. A. (1987) Cocontraction and coactivation of muscles during human gait. *IEEE 9th Ann. Conf. Engng Med. & Biol.,* pp. 1050–1051.

Winters, J. M. and Stark, L. (1985) Analysis of fundamental human movement patterns through the use of in-depth antagonistic muscle models. *IEEE Trans. biomed. Engng* **BME-32,** 826–839.

Winters, J. M. and Stark, L. (1988) Estimated mechanical properties of synergistic muscles involved in movements of a variety of human joints. *J. Biomechanics* **21,** 1027–1041.

Yamaguchi, G. T. and Zajac, F. E. (1990) Restoring unassisted natural gait to paraplegics via functional neuromuscular stimulation: a computer simulation study. *IEEE Trans. Biomed. Engng* **37,** 886–902.

Zajac, F. E. (1989) Muscle and tendon: properties, models, scaling and application to biomechanics and motor control. *CRC Crit. Rev. biomed. Engng* **17,** 359–411.